

We are IntechOpen, the world's leading publisher of Open Access books Built by scientists, for scientists

6,900

Open access books available

185,000

International authors and editors

200M

Downloads

Our authors are among the

154

Countries delivered to

TOP 1%

most cited scientists

12.2%

Contributors from top 500 universities



WEB OF SCIENCE™

Selection of our books indexed in the Book Citation Index
in Web of Science™ Core Collection (BKCI)

Interested in publishing with us?
Contact book.department@intechopen.com

Numbers displayed above are based on latest data collected.
For more information visit www.intechopen.com



Sub-Pixel Technique for Time Series Analysis of Shoreline Changes Based on Multispectral Satellite Imagery

Qingxiang Liu and John C. Trinder

Abstract

The measurement and monitoring of shoreline changes are of great interest to coastal managers and engineers. Shoreline change information can be crucial for the assessment of coastal disasters, design of coastal infrastructure and protection of coastal environment. This chapter presents shoreline change monitoring based on multispectral satellite imagery and sub-pixel technique. Firstly, a brief introduction of shoreline definitions and indicators is given. Sub-pixel techniques for shoreline mapping on multispectral satellite images are then introduced. Following that, a brief review of existing research studies of long-term shoreline change monitoring based on multispectral imagery is given. Subsequently, a case study of sub-pixel shoreline change monitoring at the northern Gold Coast on the east coast of Australia is presented. By comparing the longshore averaged beach widths at seven representative transects from Landsat with those from Argus imaging data, the RMSEs range from 9.1 to 12.3 m and the correlations are all no less than 0.7. Annual means and variabilities of beach widths were estimated without significant differences from the reference data for most of the results. Finally, conclusions and recommendations for future work are given.

Keywords: shoreline mapping, change monitoring, satellite imagery, multispectral, super-resolution mapping (SRM)

1. Introduction

1.1 Shoreline definitions and indicators

A 'Shoreline' is ideally defined as the interface between the land and water [1]. However, because of its temporally and spatially dynamic nature, the definition of shoreline should be considered in a temporal sense [2]. The shoreline is dynamic as unconsolidated sediments along the beach adjust constantly to changes of environmental forces. Sediments are deposited offshore during energetic conditions, resulting in an erosion trend of the shoreline; during calm conditions, sediments are returned back to the subaerial area, leading to an accretion of the shoreline [3]. The erosion-recovery circles may occur over several days, or as long as several decades during extreme wave conditions. In addition to shoreline changes resulting from

cross-shore sediment exchanges, along sediment exchanges can also occur, leading to relative movements between updrift and downdrift ends of the beach, which is commonly referred to as “beach rotation” [3].

For practical purposes, coastal investigators have adopted various indicators to approximate the real shoreline positions. A comprehensive literature review of shoreline definitions with extensive references is given in [2]. Three groups of shoreline indicators exist. The first group of shoreline indicators are based on visually interpreted features. A visually interpreted shoreline is a coastal feature that can be physically seen, which can change without any onshore or offshore movement of sand because it is affected by tide, wave and weather conditions [4]. Despite the definitions, some visually interpreted shoreline indicators may sometimes not be observable. For example, the high water line (HWL), which was defined as the mark left by maximum run-up from the previous high tide, may appear as a transitional zone instead of a clear line, or may not be visible at all [5]. Also, as the sand gradually dries out after previous waves, a discernible wet/dry boundary may not be available. In addition, some of the indicators are ambiguous, subjective or even inconsistent between different studies [2]. Therefore, visually interpreted shorelines may require experience and skills from the interpreters.

The second group of shoreline indicators are tidal datum-based, which are determined by the intersection of the beach profile with specific vertical tidal elevations. Generally, they are temporally and spatially more stable and are less responsive to wave condition changes than visually interpreted shorelines [4, 6, 7]. Tidal datum-based shorelines are easy to understand and less likely to be ambiguous, but their extraction requires beach profile data, i.e. 3D survey data.

The third group of shoreline indicators reported by [2] depend purely on image processing techniques and are not necessarily visually discernible. As digital image processing is more and more widely used, especially when an automatically instead of manually extracted shoreline is required, this group of shoreline indicators are not uncommon nowadays, e.g. [8–10].

The decision as to which group of shoreline indicators to use largely depends on data availability. Taking 2D satellite imagery as an example, the lack of elevation information prohibits the extraction of tidal datum-based shorelines. Also, the spatial resolution of the images significantly affects the feasibility of extracting visually discernible shorelines. Since the stabilities of these shoreline indicators are different, the decision should also take account of the investigated temporal scales, i.e. whether short-term or long-term shoreline change is of interest. In addition, a single shoreline indicator should be consistently used as possible when comparing shoreline changes over time.

1.2 Sub-pixel techniques for shoreline mapping

While shorelines are primarily linear features, the extraction using only edge detection methods can be a difficult task, because of the lack of sufficient and consistent contrast between water body and land. Besides, shorelines should be continuous and normally unique, which increases the requirements of extracting edges. In this case, shoreline mapping can be converted to the task of boundary extraction between water and land regions on a labelled map, which is produced through a classification step.

For images with medium to low spatial resolutions, pixels are most likely to be mixed. In other words, many pixels contain multiple land covers and the actual boundaries between classes generally run through the content of mixed pixels. Consequently, a traditional pixel-based classification which forces each pixel to

be assigned to a single class label may mis-locate the boundaries between classes. This mis-location will be more significant as the pixel size increases. In this case, image processing at a sub-pixel level is preferred. Sub-pixel mapping techniques, which is also referred to as super-resolution mapping (SRM), was defined as the process of spatially designating class proportions to concrete pure sub-pixels [11]. SRM aims to produce a classification map at a finer scale than the original image, under the basic assumption of spatial dependence between pixels [12]. According to [11], there are generally two steps for SRM as shown in **Figure 1**. The first step is calculating the proportion of each class inside a pixel, which is also called soft classification. The second step is spatially assigning land cover classes to pure sub-pixels according to their proportions in the pixel, after which a classification map at a finer scale is generated. Readers are referred to [11] for more details of SRM.

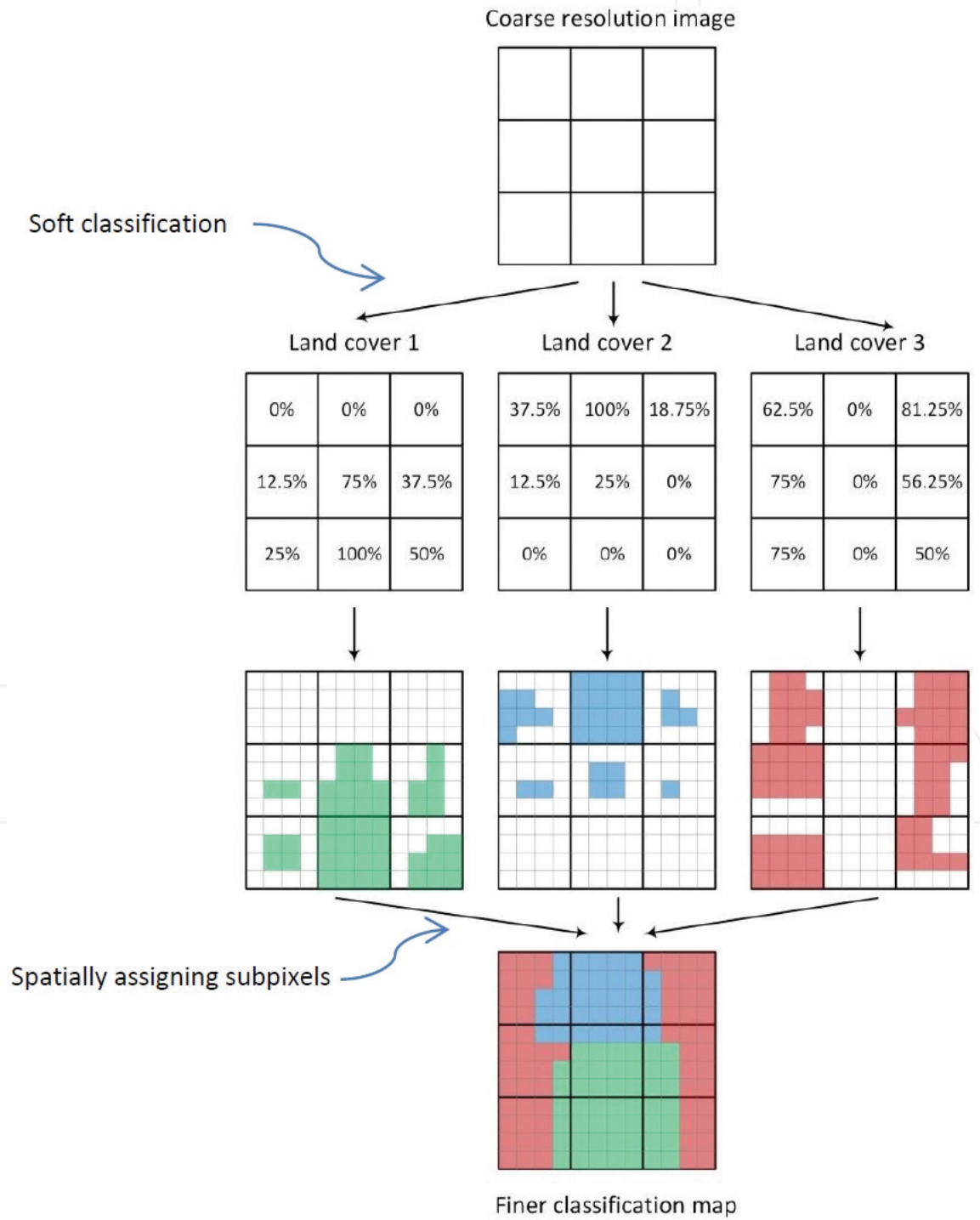


Figure 1.
SRM principle (adapted from [11, 15]).

SRM has been demonstrated in some research works (e.g. [11–14]) to be suitable for image classification at sub-pixel level.

Ref. [16] compared the performance of three SRM methods, i.e. contouring of soft classification [17], wavelet based interpolation and geo-statistical two-point histogram methods [18], for the extraction of sub-pixel shorelines from a degraded IKONOS satellite image. They used the shoreline extracted from the original IKONOS image as reference and demonstrated that all three SRM methods outperformed pixel-based classification and that the geostatistical two-point histogram method gave the best result over the study site. Ref. [19] tested two SRM methods also on a degraded IKONOS image, using both local and global training statistics. In Ref. [20] Normalised Difference Water Index (NDWI) was calculated to distinguish water and land, which was defined as

$$NDWI = \frac{B_{Green} - B_{NIR}}{B_{Green} + B_{NIR}} \quad (1)$$

where B_{Green} and B_{NIR} represent green and NIR bands of Landsat Enhanced Thematic Mapper Plus (ETM+) images respectively. Lake shorelines were then extracted at sub-pixel level based on sub-pixel edge localisation and smoothing. Using QuickBird panchromatic images as reference data, the authors demonstrated that the extracted shorelines gave a better estimation of lake areas and perimeters than pixel-based results. Ref. [9] developed a method to automatically extract sub-pixel shorelines using the near-infrared (NIR) band of Landsat images. They compared 45 sub-pixel shorelines with manually edited shorelines from aerial photos, demonstrating that the error of sub-pixel shoreline locations over their study site is less than 6 m. All of these above mentioned studies indicate that SRM techniques can be effective for improving shoreline mapping accuracy on medium to low-resolution satellite images.

1.3 Long-term shoreline change monitoring using multispectral satellite images

Since most of the high-resolution satellites were launched no earlier than two decades ago, they are mostly not suitable for monitoring long-term (e.g. multi-decadal) shoreline changes. Therefore, most of the studies in the literature used medium to low-resolution satellite data such as Landsat, ASTER and SPOT imagery as the main data source, e.g. [21–23].

The Landsat program dates back to 1972, producing multi-decadal archival data freely available to the public with a revisit time of 16 days since Landsat-4. Although a number of case studies on using Landsat data to monitor long-term shoreline changes exist, there are a limited number of existing long-term coastal monitoring programs producing ground-truth data with both high spatial and temporal resolutions [24, 25]. The availability of ground-truth data is likely to have limited the amount and temporal frequency of experimental data used in the literature. Most of the studies have used only a small percentage of available archival Landsat satellite images with yearly frequency or even longer time intervals, e.g. [26–28]. Only a few studies have used a frequency higher than yearly [9, 29] or even all the available Landsat data [30, 31] over the studied areas. However, the ground truth data used in these studies was either over a much shorter term [30] or much lower than monthly frequency [31]. Consequently, intra-annual variability over a long term may not be revealed and validated. Ref. [10] presented a case study of using full-frequency archival Landsat data for monitoring of shoreline changes during approximately three decades, where long-term and temporally dense ground surveying data is used as reference data.

2. Long-term shoreline change monitoring: a case study at the northern Gold Coast, Australia

2.1 Study site description

The Gold Coast is a coastal city located approximately 66 km southeast of Brisbane near the Queensland-New South Wales state border (**Figure 2(b)** and (c)). The Gold Coast comprises a 35 km-long east-facing shoreline of over a dozen of beaches, stretching from the Rainbow Bay at the southern end to South Stradbroke Island in the north. The study area is a part of the northern Gold Coast between Main Beach and Broadbeach (**Figure 2(a)**), extending 4.5 km alongshore.

The Gold Coast beaches are characterised as energetic, intermediate beaches with mean offshore significant wave height and peak wave period of 1.1 m and 9.4 s respectively [32]. Beach sediments of the site have a mean grain size of 0.25 mm and a fall velocity of around 0.03 m/s. Tides in this area are micro-tidal and semidiurnal with a mean spring tidal range of approximately 1.8 m. Waves are predominantly from the southeast and show strong seasonal variations, with larger waves and more frequent storms during Australian summer to fall months (i.e. December to June) while milder waves occur during winter and spring months [32]. The nearshore morphology of the study site is characterised as a double sandbar system with a nearshore bed slope around 0.02 [33]. The net longshore drift is estimated to be 500,000 m³ per year northwards [32]. This study site is an open, straight sandy beach, which is a representative of moderate to high wave energy, wave-dominated (micro-tidal) beaches.

2.2 Northern Gold Coast Beach protection strategy

The Gold Coast is a major tourist destination that offers some of the most popular surfing beaches in Australia. However the tourist economy is at risk of

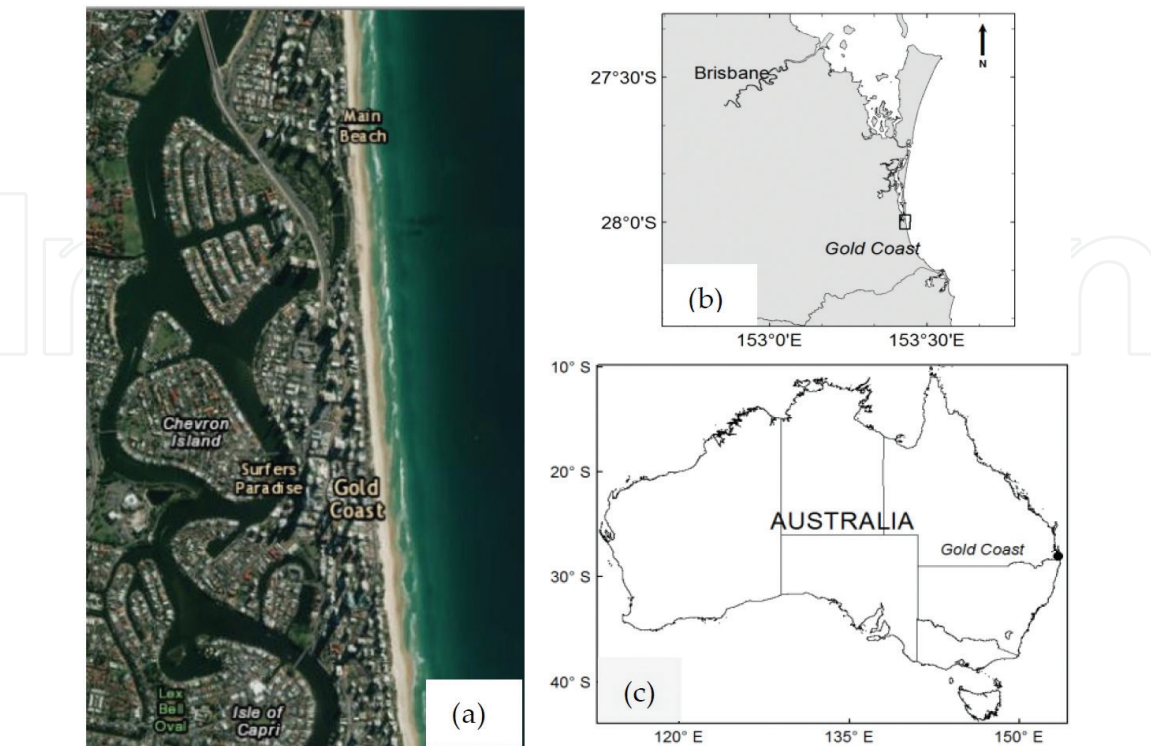


Figure 2.
(a) Study site: the northern Gold Coast (source: ArcMap basemap). (b) The location of Gold Coast with respect to Brisbane. The study area is marked as the small black rectangle. (c) The location of Gold Coast in the map of Australia.

significant losses due to beach erosion during major storm events. The Northern Gold Coast Beach Protection Strategy (NGCBPS) was a long-term, sustainable plan to maintain and enhance the beaches at the northern Gold Coast [34]. As a part of the NGCBPS, over 1.2 million cubic metres of sediment were deposited on the northern Gold Coast beaches and within the nearshore to increase beach amenity and widen the beaches as preparation for future storm events. The locations of the six sand nourishment deposition areas A1 to A6 are indicated in **Figure 3(a)**.

The beach nourishment program was commenced in February 1999 and the major phase was completed in June 2000. The progress of the nourishment is shown in **Figure 3(b)**, where the cumulative nourishment volumes at the six deposition areas are indicated using different grey scales. Note that A1a is an area approximately 300 m north of A1 and is not shown in **Figure 3(a)**. In addition, a submerged artificial reef (marked as a blue circle in **Figure 3(a)**) was built within the nearshore at Narrowneck primarily to stabilise the beach nourishment and improve surfing quality, which was initiated approximately a half year later than the commencement of the beach nourishment (in August 1999). The main phase of the reef construction was completed in December 2000.

2.3 Data used

2.3.1 Reference shorelines

Funded by the City of Gold Coast, an Argus coastal monitoring system was installed in late July 1999 at the northern Gold Coast by the Water Research Laboratory (WRL), University of New South Wales to monitor shoreline changes. Four video cameras were installed approximately 100 m above the ground on the

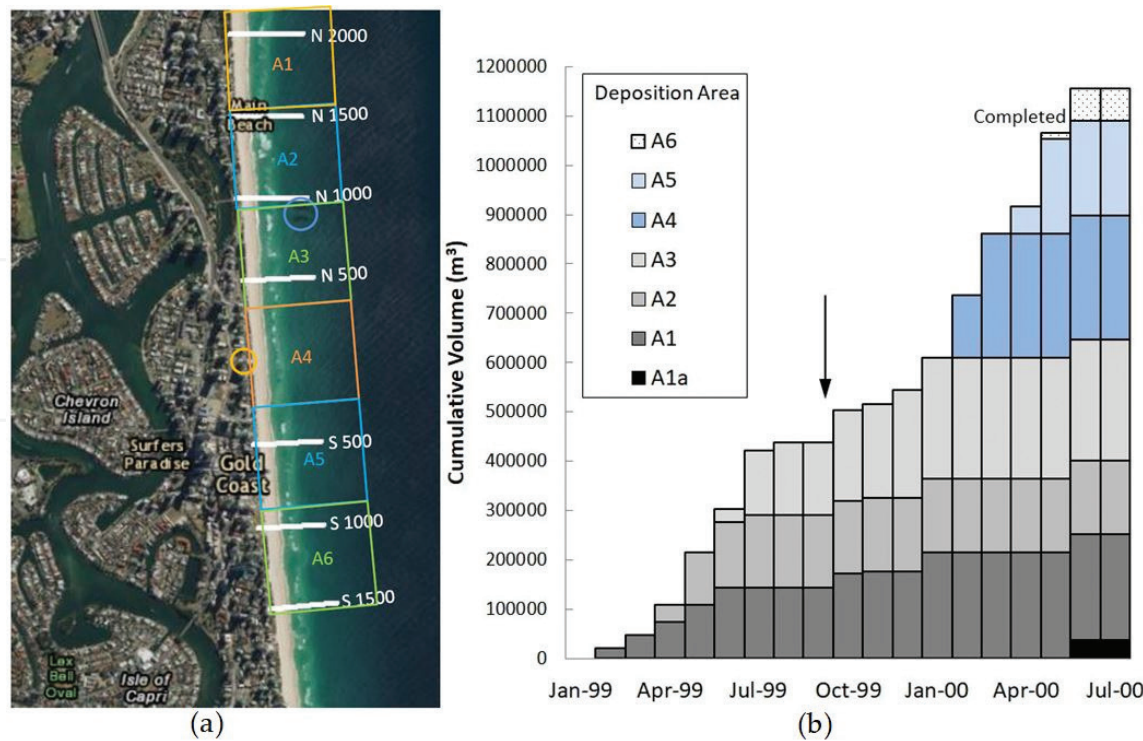


Figure 3.
(a) Locations of sand nourishment deposition areas A1 to A6 (marked as squares). The locations of the focus building where the Argus cameras were installed and the artificial reef at Narrowneck are marked as orange and blue circles respectively. The locations of the seven regularly spaced cross-shore profile lines, i.e. from 2000 m north (N 2000) to 1500 m south (S 1500) of the Argus station are also indicated. (b) Progress of sand nourishment (adapted from [35]) at all deposition areas. The black arrow indicates the time when the Argus coastal monitoring was initiated.

Focus Building, which is located about 60 m landward of the dune line and 900 m to the south of Narrowneck (**Figure 3(a)**). The system became fully operational in August 1999, which coincided with the commencement of Narrowneck reef construction. The Argus monitoring project lasted from 1999 to 2008 and was recommenced in 2014.

Every daylight hour, the cameras collected a 10-minute time-averaged image, from which the natural variations of breaking waves were effectively averaged. To minimise the effects of tidal variations, only the time-averaged images acquired at mid-tide, which is approximately 0 m on the Australian Height Datum (AHD) were selected. Among the selected images, only those acquired when the root-mean-square wave heights were no more than 1 m were retained for future use. These images were rectified and geo-referenced through a standardised image pre-processing procedure [35]. Shorelines were then extracted by WRL staff using the pixel intensity clustering (PIC) method [8, 36]. The shoreline positions were defined as the cross-shore locations of the mean sea level contours [37] and may not be visually discernible on the time-averaged video images. Therefore, they are believed to belong to the third group of shoreline indicators and depend on the PIC method. It is estimated that the horizontal errors of the extracted shoreline time-series were within ± 5 m [37]. While the nominal frequency of the shorelines is weekly [35], the actual frequency depends on the wave conditions during the monitoring period. During the studied period (1999 to 2008), the average time frequency of available shorelines is 6–9 days.

2.3.2 Experimental Landsat images

Decided by the availability of the reference data, Landsat multispectral images spanning approximately 9 years, i.e. from August 1999 to October 2008 were used. The dataset consists of images acquired by two satellite instruments—Landsat 5 Thematic Mapper (TM) and Landsat 7 ETM+. For Landsat 7 ETM+ instrument, the products before and after the scan line corrector (SLC) failure are used. Surface Reflectance products which have been atmospherically corrected based on L1T (precision terrain) data were ordered from U.S. Geological Survey (USGS) website <https://espa.cr.usgs.gov/>. Radiometric calibration and cross-calibration have been implemented [38] by USGS. As reported by NASA, the geo-registration errors are within 0.4 pixels (12 m), indicating the variation in position between images at different times is at subpixel level. The numbers and spanning periods of images used, after eliminating scenes blocked by thick clouds, are indicated as **Table 1**.

2.4 Shoreline extraction from Landsat images

The shoreline extraction and change monitoring flow chart is described as **Figure 4**. Firstly, Landsat images were clipped based on the boundary of the study site. A simple one-dimensional cubic interpolation was employed to fill the gaps on the Landsat 7 images in SLC-off mode. This step was merely for extracting continuous shorelines and the interpolated values were not utilised for beach widths calculation. Then, shorelines at sub-pixel level were extracted from the nine-year Landsat data using the strategy illustrated in [10]. Due to the limitation of the spatial resolution of Landsat images, the extracted shorelines are not visually discernible. Therefore, these shorelines also belong to the third group of shoreline indicators and depend on the shoreline extraction strategy.

Subsequently, tidal correction was applied to the shorelines extracted from Landsat images. Assuming the beach face slope did not vary significantly alongshore, which is a valid judgement from the averaged historical ground measurements, the horizontal and cyclic translation of the shoreline caused by tidal variation can be simplified as

$$\Delta = Z/m,$$

(2)

where Δ is the horizontal cross-shore shift; z is the tidal elevation at image acquisition time relative to 0 m AHD. Astronomical tidal elevations recorded every 15 minutes at the nearest available location of Southport (approximately 3 km from the Focus Building) were used for tidal correction. An intertidal beach face slope of 0.06, which is the mean beach slope between 0 and 2 m AHD at Narrowneck [39] was used for the correction.

	TM	ETM+ (SLC-on)	ETM+ (SLC-off)
Period	1999–2008	1999–2003	2003–2008
Number of scenes	63	53	61

Table 1.
Description of Landsat multispectral data used.

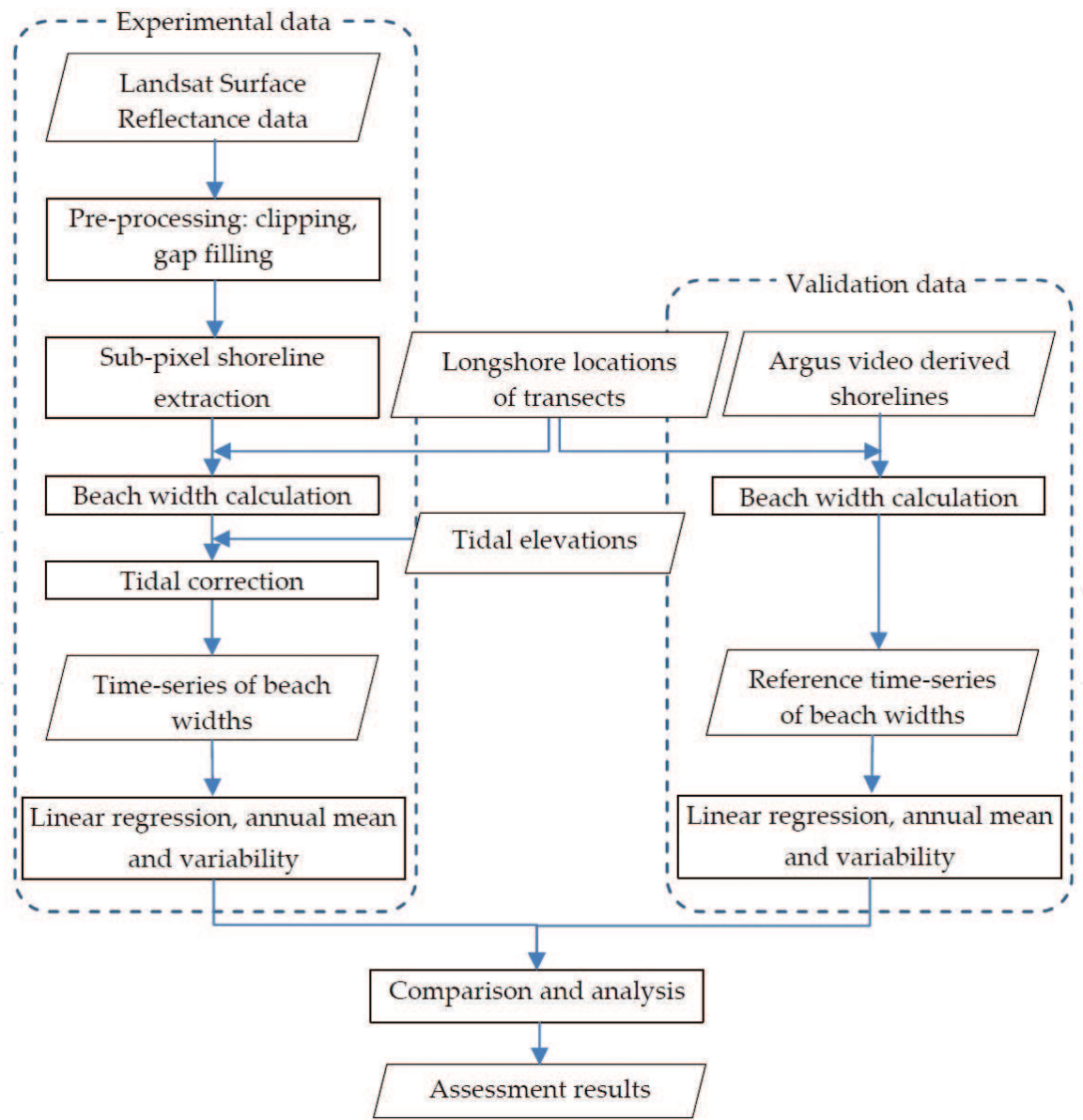


Figure 4.
Flow chart of shoreline mapping and change monitoring.

2.5 Results and discussions

2.5.1 Time-series beach width results

Based on the shorelines derived from Landsat and video imaging data, 100 m longshore-averaged beach widths centred at seven representative transects (marked in **Figure 3(a)**) were calculated. These transects were spaced at a regular interval of 500 m, i.e., they are 2000, 1500, 1000, 500 m to the north, and 500, 1000, 1500 m to the south of the Argus cameras. The selected alongshore locations are consistent with [35] as the report indicated that beach widths at these transects are suitable for the analysis of shoreline trends and variabilities. Using longshore averaged beach widths aims to average out the effects of the longshore varied instantaneous waves at the beach face. The area nearest to the cameras (0 m alongshore) was not selected because of sun glint and the gap between the field views of the cameras [35].

Figure 5 shows the time-series beach widths from 1999 to 2008 at the seven transect lines after tidal correction, compared with video imaging derived results (as reference data). The legend for the alongshore locations were abbreviated according to whether they were north (N) or south (S) followed by their distances, relative to the Argus cameras, e.g. 2000 m at the north was abbreviated as N 2000 and 1500 m at the south as S 1500. The time-series beach widths at the seven locations show very similar trends in the results from the Landsat data compared with the reference data, despite some intermittent results with noticeable errors. The beach widths over the 9 years along the full 4.5 km study area can be seen to have varied up to approximately 100 m.

To realise pairwise comparisons between Landsat and video imaging derived beach widths, each of the final ground truth beach widths was calculated using a linear interpolation between the closest pair of pre and post surveys corresponding to each satellite image acquisition time. A time-series of errors was derived at each transect location as the difference between each pair of Landsat and video imaging derived beach widths. Subsequently, the mean error (ME), mean absolute error (MAE) and root mean squared error (RMSE) of the time-series results from Landsat were calculated as listed in **Table 2**.

2.5.2 Annual mean and variability

Annual mean beach widths from 2000 to 2008 at the seven profile lines were calculated for both Landsat and Argus video imaging based results shown as **Figure 6**. Note that year 1999 was excluded since the available video-based data for that year spanned less than half a year. The inter-annual shoreline change trends derived from Landsat match very well with those from video imaging data, with the most noticeable discrepancies at the northern part during 2000–2003. It was found that during those years the average frequency of the ground survey data and/or the Landsat data at the northern part of the beach (N 2000–N 500) was much lower than average. Taking year 2000 as an example, the average frequencies of the ground survey and Landsat data at the northern part were approximately 17 and 35 days respectively. This is believed to be the main reason for the significant divergence between the annual means of Landsat and ground survey data during that period, as it is believed that higher-frequency data would lead to more accurate estimations of annual mean beach widths.

Table 3 presents the statistical assessment of annual mean beach widths at the seven locations, where the RMSEs are in the range of 3.9–7.2 m. Statistical t-tests of the beach width results from Landsat and video imaging within each year of 2000–2008 were employed, there being nine tests for each of the seven locations. The majority of the tests

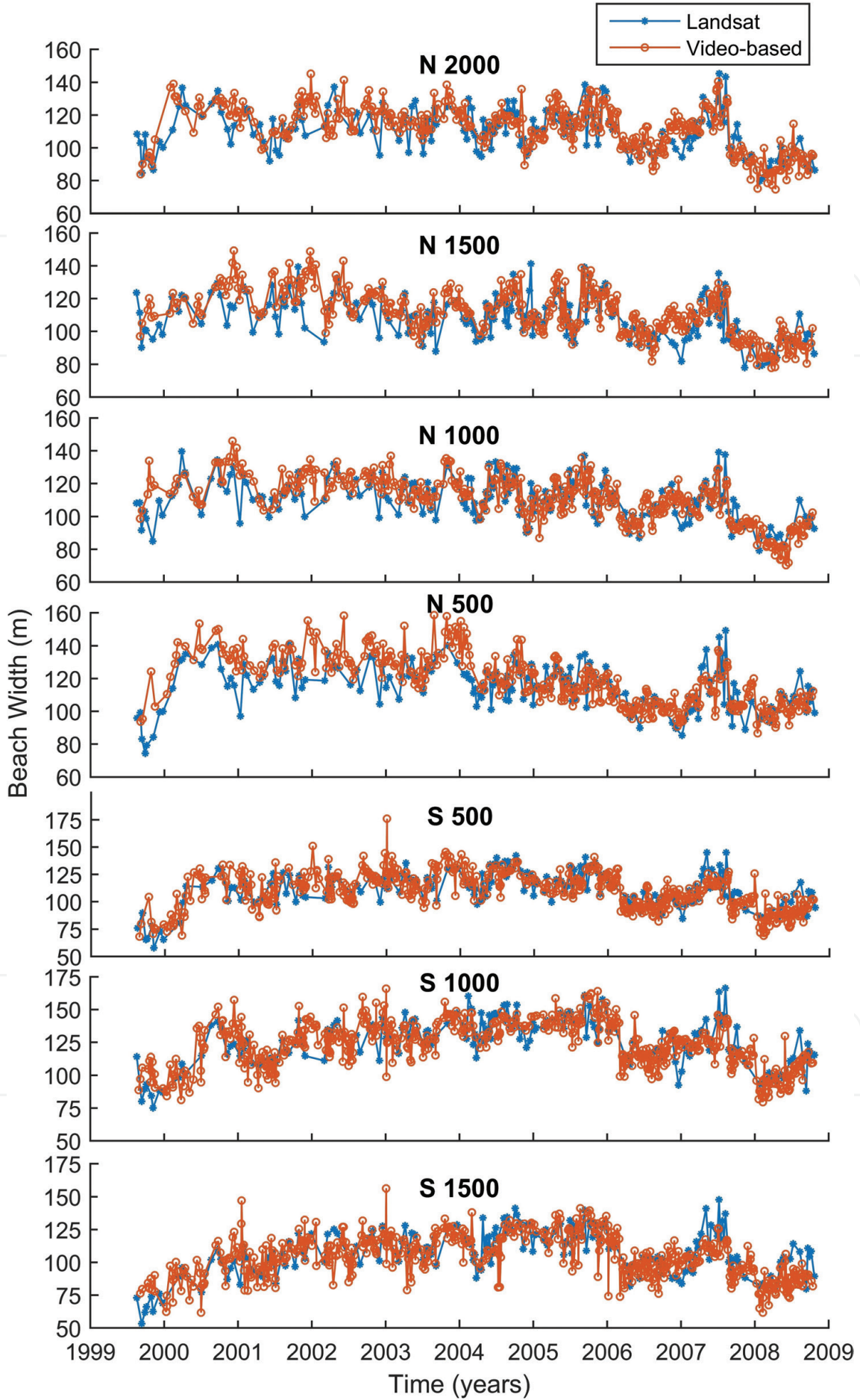


Figure 5. Time-series beach widths along the seven transects at northern Gold Coast from August 1999 to October 2008. Blue and orange curves represent beach widths from Landsat and Argus coastal video imaging data respectively.

	N 2000	N 1500	N 1000	N 500	S 500	S 1000	S 1500
ME (m)	−1.5	−3.2	−1.0	−4.0	0.0	0.1	1.6
MAE (m)	7.7	8.0	7.2	8.9	9.1	8.8	9.7
RMSE (m)	9.6	10.2	9.1	11.1	11.7	11.4	12.3
Correlation	0.71	0.71	0.72	0.70	0.73	0.78	0.73

Table 2.
Statistical assessment of full time-series beach widths at the seven profile locations.

did not reject the null hypothesis of no significant difference at 5% significance level where only 16 out of the 63 tests rejected the null hypothesis. This indicates the suitability of Landsat data for monitoring annual mean shoreline behaviour at the study site.

The standard deviations within each of the 9 years for the seven locations were calculated and displayed in **Figure 7**. Intra-annual variabilities derived from Landsat data do not appear consistently larger or smaller than the video-based measurements at the northern Gold Coast. The F-test was employed within each of the 9 years to statistically compare beach width variances derived from Landsat and video imaging data. The great majority of tests did not reject the null difference hypothesis of no differences at the confidence level of 95%, where only 6 out of the 63 tests rejected the null hypothesis. This indicates that Landsat data can produce consistent estimations of annual variances with the reference data at the study area.

2.5.3 Shoreline change trends

2.5.3.1 Effects of beach nourishment

It is believed worthwhile to explore the capability of Landsat data to identify the beach width changes predominantly affected by the beach nourishment that occurred between 1999 and 2000. Observing the beach widths (**Figure 8**) from both Landsat and video imaging data during the first year of monitoring (when the nourishment was ongoing), it is clear that the beach widths at the northern part started to show an increase trend soon after the commencement of Argus monitoring project, which is especially observable at N 2000 and N 500. In contrast, the beach widths at the southern part did not show increasing trends until early 2000 when the nourishment at A4–A6 was started. In other words, the time lag of beach widening between the northern and southern parts of the study area as the beach nourishment progressed southwards is observable.

Linear regressions were applied separately to the time-series beach widths from both Landsat and video imaging data from August 1999 to July 2000 and afterwards. The linearly fitted lines are superimposed on the plotted original time-series beach widths in **Figure 8**. The fitted lines at both north and south of the study area show clear increasing trends during August 1999 to July 2000. The regressed changing rates are listed in **Table 4**, which are all positive except for the change rate calculated from video imaging data at N 1000.

Since single beach width results from Landsat data may be erroneous and the time frequency of the extracted shorelines is relatively low, Landsat-estimated linear changing rates during such short periods (i.e. only approximately 1 year) are not reliable, as indicated by the significant differences of the regression rates between Landsat and video imaging results at most of the seven locations. Nevertheless, the most significant accretion rates are at N 2000, N 500 and S 500 for both Landsat and video imaging results. This is consistent with the progress of the nourishment (**Figure 3(b)**) since additional sand was deposited in A1 and A3 (where transects

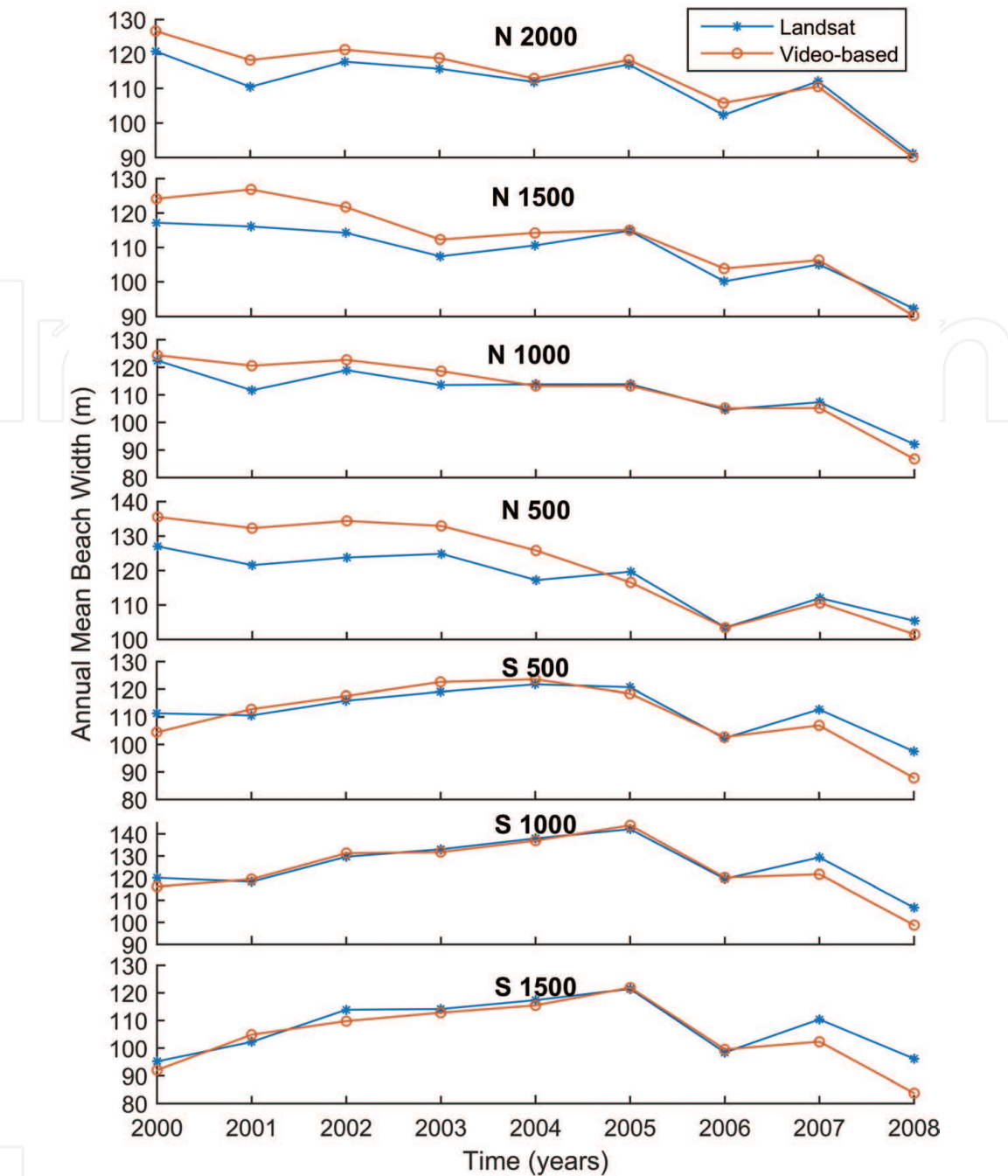


Figure 6. Annual mean beach widths at the seven locations at northern Gold Coast. Blue and orange curves represent annual mean beach widths from Landsat and from video imaging data respectively.

	N 2000	N 1500	N 1000	N 500	S 500	S 1000	S 1500
ME (m)	−2.6	−4.1	−1.3	−4.3	1.6	1.9	2.9
MAE (m)	3.2	4.6	3.2	6.1	3.8	3.1	3.9
RMSE (m)	3.9	5.6	4.2	7.2	4.7	4.2	5.3

Table 3. Statistical assessment of annual mean beach widths at the seven locations.

N 2000 and N 500 were located) during the first year of the coastal monitoring, although a large volume of sand had already been deposited before the monitoring commenced. Besides, the sand nourishment at A5, where transect S 500 was located, was implemented after the commencement of the Argus monitoring. In contrast, the nourishment of A2, where transects N 1500 and N 1000 are located,

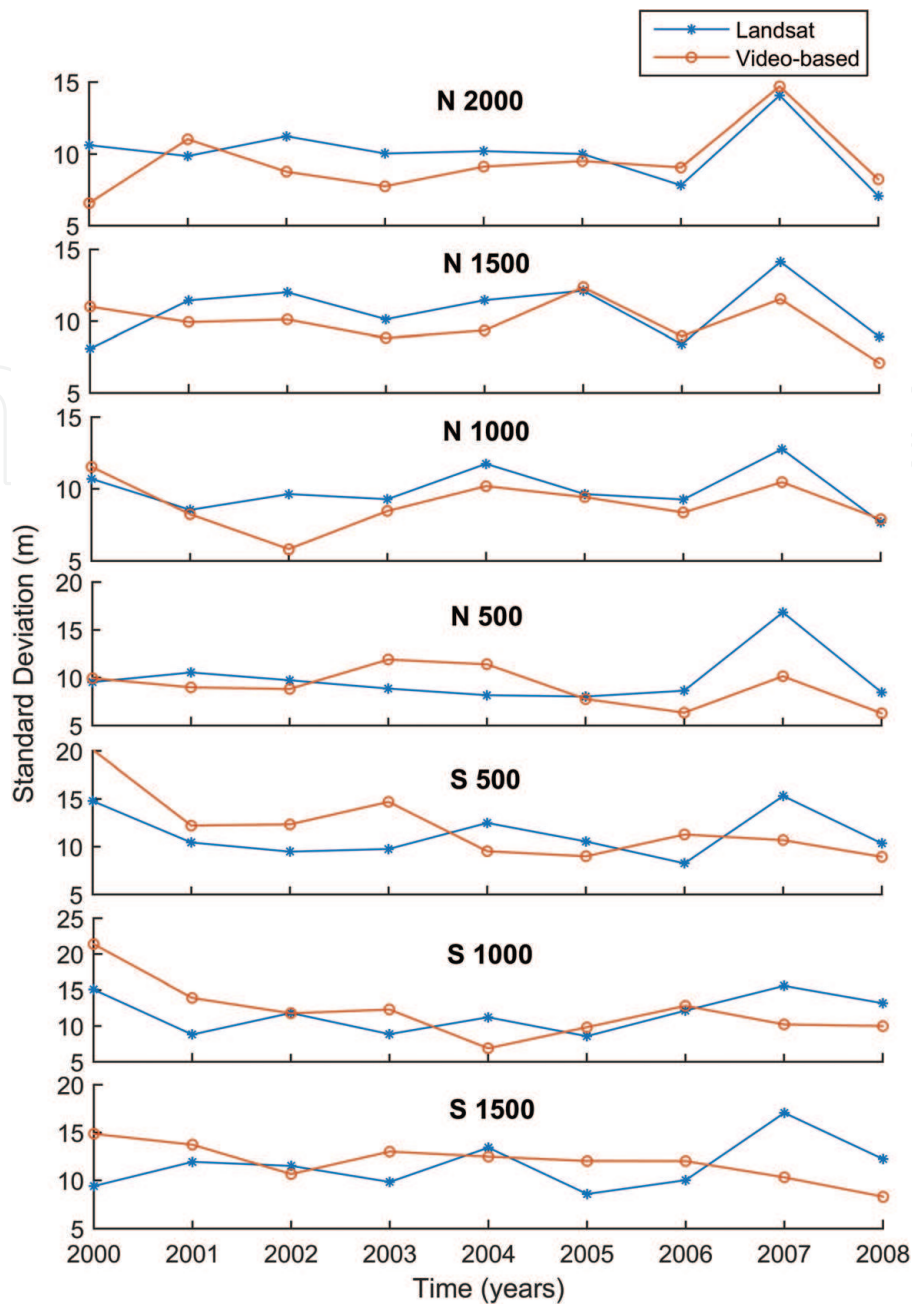


Figure 7. Annual standard deviations of beach widths at the seven locations at northern Gold Coast. Blue and orange curved represent annual standard deviations from Landsat and coastal video imaging data respectively.

had been completed several months before the coastal monitoring program, and the beach widths over that area are expected to have increased before August 1999. The linear regression results indicate that the effects of beach nourishment progress can be statistically identified from Landsat data.

2.5.3.2 Shoreline change trends post beach nourishment

To quantify the overall trends post beach nourishment at the seven locations, linear regressions were also applied to the time-series results from Landsat and reference data from August 2000 onwards. Slightly decreasing trends were observed at all locations (see the regression lines in **Figure 8**) and corresponding negative changing rates (**Table 4**) were derived from both Landsat and reference data, indicating overall modest erosion trends post the beach nourishment.

Observing **Figure 9** and based on the analysis of shoreline changes illustrated in [35], the post beach nourishment period was judiciously divided into four shorter

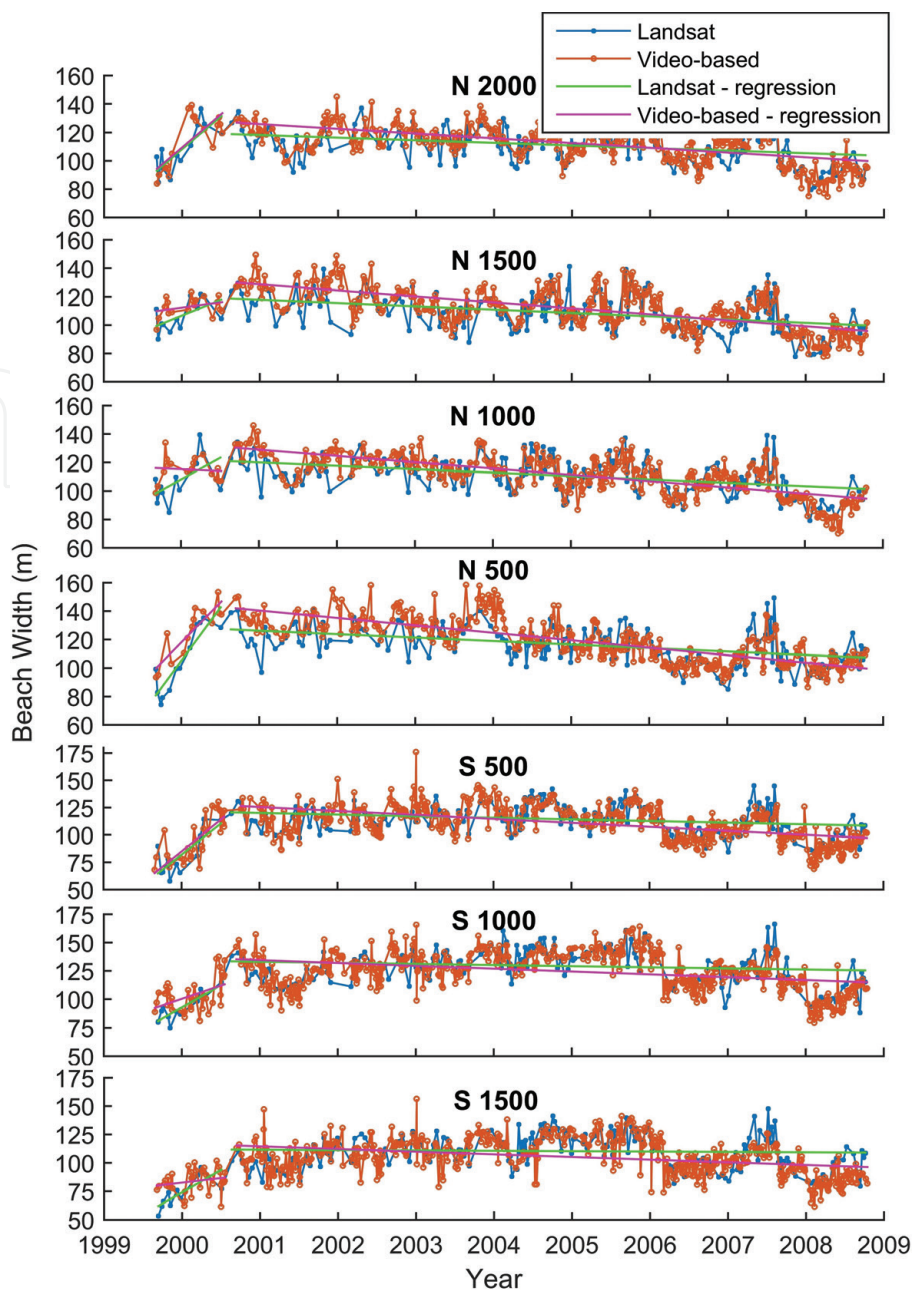


Figure 8. Linear regression lines of beach widths at the seven profile locations during and after the beach nourishment, where the original time-series of beach widths from Landsat (blue curves) and video imaging data (orange curves) are also plotted for reference.

		N	N	N	N	S	S	S
		2000	1500	1000	500	500	1000	1500
Aug 1999–Jul 2000	Landsat	46.6	22.3	30.3	74.4	56.3	39.0	39.4
	Reference	46.9	7.6	−2.5	55.9	58.4	22.7	8.0
Aug 2000–Oct 2008	Landsat	−1.8	−2.3	−2.4	−2.4	−1.5	−1.0	−0.3
	Reference	−3.3	−4.2	−4.4	−5.2	−3.6	−2.5	−2.3

Table 4. Shoreline changing rates (m/year) of beach widths at the seven locations during and post beach nourishment.

periods: August 2000–February 2006, March 2006–July 2007, August 2007–January 2008 and February 2008–October 2008. Linear regressions were applied to the beach widths during each of the periods and the regression lines are displayed in **Figure 9**.

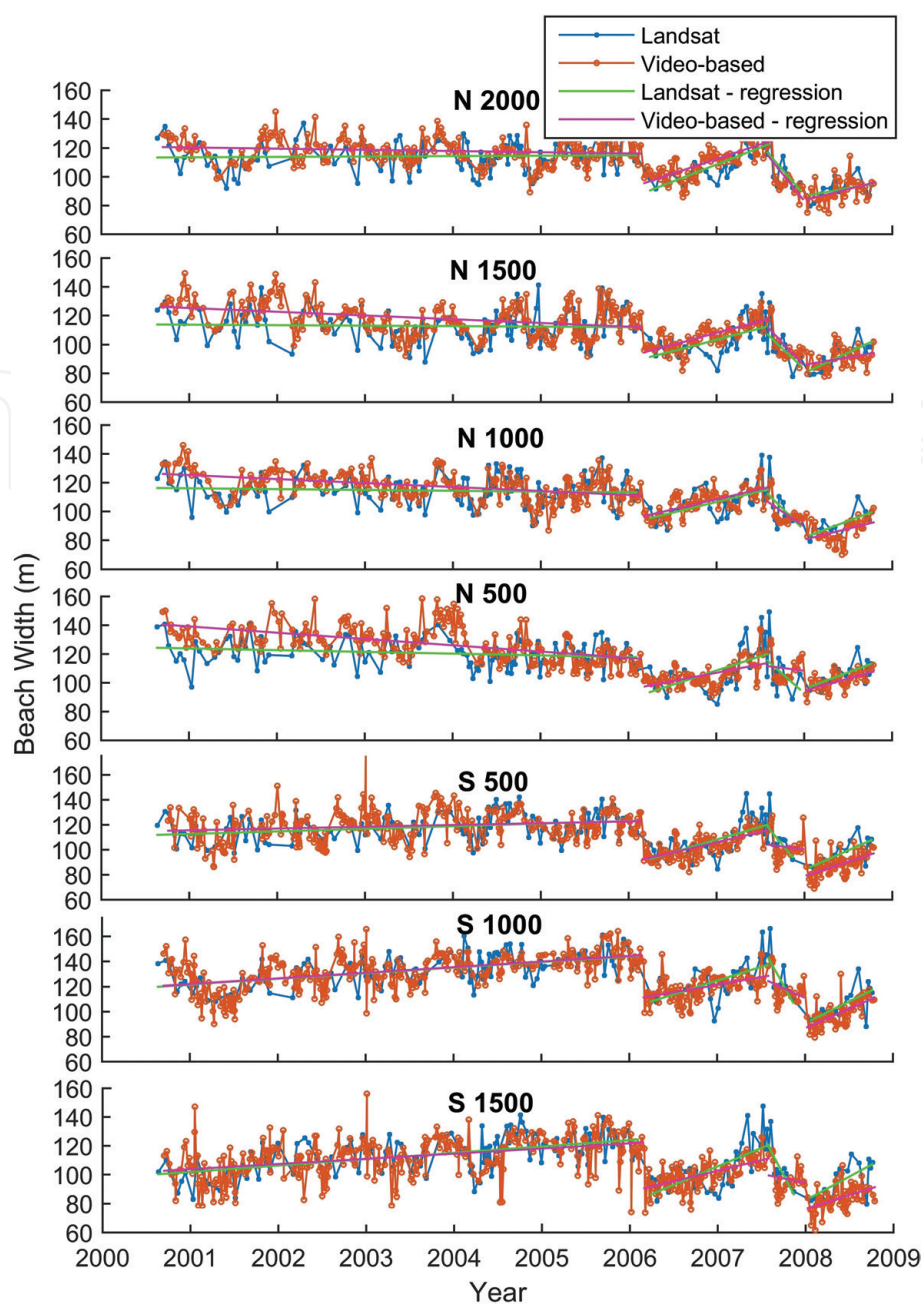


Figure 9. Linear regressed shoreline change trends during shorter periods post beach nourishment at the seven locations, where the original time-series of beach widths post beach nourishment from Landsat (blue curves) and video imaging data (orange curves) are also plotted for reference.

		N 2000	N 1500	N 1000	N 500	S 500	S 1000	S 1500
Aug 2000– Feb 2006	Landsat	0.28	−0.3	−0.6	−1.2	2.1	4.5	4.4
	Reference	−0.8	−2.6	−2.8	−4.4	1.4	4.5	3.6
Mar 2006– Jul 2007	Landsat	24.8	18.0	15.7	21.8	22.3	20.9	26.1
	Reference	20.6	16.1	14.5	11.2	16.6	11.5	14.5
Aug 2007– Jan 2008	Landsat	−72.7	−77.4	−65.1	−72.7	−121.3	−119.0	−119.5
	Reference	−72.4	−60.4	−39.5	−0.9	−3.8	−25.3	−4.8
Feb 2008– Oct 2008	Landsat	11.0	28.4	22.8	22.9	31.2	34.4	32.9
	Reference	15.2	10.4	15.2	17.1	23.0	30.9	18.7

Table 5. Shoreline changing rates (m/year) during shorter periods post beach nourishment at the seven locations using linear regression.

The corresponding changing rates during those periods are given in **Table 5**. During the period from August 2000 to February 2006, the northern parts of the study area generally exhibited slight erosions, whereas the southern parts showed modest accretion trend. Dramatic erosions can be clearly observed at all locations in March 2006, as a result of relatively slow passage of an east coast low pressure weather system [35]. In the following months until July 2007, the beach had a steady recovery trend at all locations. During the last period (February to October 2008), the entire beach showed consistent recovery trends.

Note that given such short periods (e.g. less than 6 months), the estimations of net erosion/accretion rates from Landsat are not reliable, as indicated by some significant differences of the regression rates between Landsat and video imaging results. However, the identified trends, i.e. whether accretions or erosions, are still mostly consistent with those from the reference data. This demonstrates the capability of Landsat data to estimate general erosion/accretion trends during periods as short as half a year.

3. Conclusions and recommendation

This chapter presents the application of multispectral satellite imagery for shoreline mapping and change monitoring. Firstly, a brief introduction of shoreline definitions and indicators is given, which is fundamental for shoreline extraction and monitoring. Next, a brief introduction of SRM techniques is presented. A brief review of existing research on time-series shoreline change monitoring based on multi-temporal multispectral satellite imagery is then presented. Most of the studies in the literature used medium to low-resolution satellite data such as Landsat, ASTER and SPOT imagery as the main data source.

Subsequently, a case study of using approximately 9 years of Landsat archival data to monitor shoreline changes at the northern Gold Coast, Australia is presented. By comparing the longshore averaged beach widths at seven representative transects from Landsat with those from Argus imaging data, the derived errors of extracted shorelines are at a sub-pixel level. Specifically, the RMSEs of beach widths at these locations range from 9.1 to 12.3 m and the correlations are all no less than 0.7; the RMSEs of annual mean beach widths are in the range of 3.9–7.2 m. Besides, annual means and variabilities of beach widths can be estimated from Landsat data, without significant differences from the reference data for most of the results. In addition, linear regression results show that Landsat data can be used to identify the general trends of beach widths, i.e. erosion or accretion, during periods as short as half a year. More importantly, beach widening as a result of the sand nourishment can be clearly observed. This case study, together with the existing work in Narrabeen-Collaroy Beach [10], further demonstrates the suitability of Landsat images for long-term shoreline change monitoring and the practicability of the super-resolution shoreline extraction strategy.

On the other hand, Landsat images can be unreliable for the monitoring of shoreline changes during much shorter periods, e.g. only a few days which is the typical duration for a coastal storm event. In this case, satellite images with both higher spatial and temporal resolutions are needed. While Landsat archival data are used in this chapter as a representative data source of medium-resolution satellite data, it is recommended that other multispectral satellite images such as the freely available Sentinel multispectral images could also be investigated.

Conflict of interest

The authors declare no conflict of interest.

IntechOpen


IntechOpen

Author details

Qingxiang Liu* and John C. Trinder
School of Civil and Environmental Engineering, University of New South Wales,
Sydney, Australia

*Address all correspondence to: qingxiang.liu@unswalumni.com

IntechOpen

© 2018 The Author(s). Licensee IntechOpen. This chapter is distributed under the terms of the Creative Commons Attribution License (<http://creativecommons.org/licenses/by/3.0>), which permits unrestricted use, distribution, and reproduction in any medium, provided the original work is properly cited. 

References

- [1] Dolan R, Hayden BP, May P, May S. The reliability of shoreline change measurements from aerial photographs. *Shore and Beach*. 1980;**48**(4):22-29
- [2] Boak EH, Turner IL. Shoreline definition and detection: A review. *Journal of Coastal Research*. 2005;**21**(4):688-703
- [3] Harley M, Turner I, Short A, Ranasinghe R. A reevaluation of coastal embayment rotation: The dominance of cross-shore versus alongshore sediment transport processes, Collaroy-Narrabeen Beach, Southeast Australia. *Journal of Geophysical Research: Earth Surface*. 2011;**116**(F4)
- [4] Ruggiero P, Kaminsky GM, Gelfenbaum G. Linking proxy-based and datum-based shorelines on a high-energy coastline: Implications for shoreline change analyses. *Journal of Coastal Research*. 2003;**(38)**:57-82
- [5] Crowell M, Leatherman SP, Buckley MK. Historical shoreline change: Error analysis and mapping accuracy. *Journal of Coastal Research*. 1991;**7**(3):839-852
- [6] Moore LJ, Ruggiero P, List JH. Comparing mean high water and high water line shorelines: Should proxy-datum offsets be incorporated into shoreline change analysis. *Journal of Coastal Research*. 2006;**22**(4):894-905
- [7] Minogue MJ. Regional-scale coastal response to the April 2015 storm using aerial photography [Honours thesis]. The University of New South Wales; 2016
- [8] Aarninkhof SG, Turner IL, Dronkers TD, Caljouw M, Nipius L. A video-based technique for mapping intertidal beach bathymetry. *Coastal Engineering*. 2003;**49**(4):275-289
- [9] Pardo-Pascual JE, Almonacid-Caballer J, Ruiz LA, Palomar-Vázquez J. Automatic extraction of shorelines from Landsat TM and ETM+ multi-temporal images with subpixel precision. *Remote Sensing of Environment*. 2012;**123**:1-11
- [10] Liu Q, Trinder J, Turner IL. Automatic super-resolution shoreline change monitoring using Landsat archival data: A case study at Narrabeen-Collaroy Beach, Australia. *Alberta Personal Property Registry Electronic System*. 2017;**11**(1):016036
- [11] Mertens K. Towards Sub-Pixel Mapping: Design and Comparison of Techniques. [S.l.: s.n.]. Ghent, Belgium: Ghent University; 2008
- [12] Mertens KC, de Baets B, Verbeke LPC, de Wulf RR. A sub-pixel mapping algorithm based on sub-pixel/pixel spatial attraction models. *International Journal of Remote Sensing*. 2006;**27**(15):3293-3310
- [13] Mertens KC, Verbeke LPC, Westra T, De Wulf RR. Sub-pixel mapping and sub-pixel sharpening using neural network predicted wavelet coefficients. *Remote Sensing of Environment*. 2004;**91**(2):225-236
- [14] Tatem AJ, Lewis HG, Atkinson PM, Nixon MS. Super-resolution land cover pattern prediction using a Hopfield neural network. *Remote Sensing of Environment*. 2002;**79**(1):1-14
- [15] Liu Q, Trinder J, Turner I. A comparison of sub-pixel mapping methods for coastal areas. *ISPRS Annals of the Photogrammetry, Remote Sensing and Spatial Information Sciences*. 2016;**III**-7:67-74

- [16] Foody GM, Muslim AM, Atkinson PM, editors. Super-resolution mapping of the shoreline through soft classification analyses. In: IGARSS 2003 2003 IEEE International Geoscience and Remote Sensing Symposium Proceedings (IEEE Cat No03CH37477). Toulouse, France: IEEE. 2003;6:3429-3431
- [17] Foody GM. The role of soft classification techniques in the refinement of estimates of ground control point location. *Photogrammetric Engineering and Remote Sensing*. 2002;68(9):897-904
- [18] Atkinson PM. Super-resolution land cover classification using the two-point histogram. In: Sanchez-Vila X, Carrera J, Gómez-Hernández JJ, editors. *geoENV IV—Geostatistics for Environmental Applications: Proceedings of the Fourth European Conference on Geostatistics for Environmental Applications Held in Barcelona, Spain, November 27-29, 2002*. Dordrecht, The Netherlands: Springer; 2004. pp. 15-28
- [19] Muslim AM, Foody GM, Atkinson PM. Localized soft classification for super-resolution mapping of the shoreline. *International Journal of Remote Sensing*. 2006;27(11):2271-2285
- [20] Shah CA. Automated Lake shoreline mapping at subpixel accuracy. *IEEE Geoscience and Remote Sensing Letters*. 2011;8(6):1125-1129
- [21] Addo KA, Jayson-Quashigah P, Kufogbe K. Quantitative analysis of shoreline change using medium resolution satellite imagery in Keta, Ghana. *Marine Science*. 2011;1(1):1-9
- [22] Chen W-W, Chang H-K. Estimation of shoreline position and change from satellite images considering tidal variation. *Estuarine, Coastal and Shelf Science*. 2009;84(1):54-60
- [23] Maiti S, Bhattacharya AK. Shoreline change analysis and its application to prediction: A remote sensing and statistics based approach. *Marine Geology*. 2009;257(1):11-23
- [24] Harley MD, Turner IL, Short AD, Ranasinghe R. Assessment and integration of conventional, RTK-GPS and image-derived beach survey methods for daily to decadal coastal monitoring. *Coastal Engineering*. 2011;58(2):194-205
- [25] Turner IL, Harley MD, Short AD, Simmons JA, Bracs MA, Phillips MS, et al. A multi-decade dataset of monthly beach profile surveys and inshore wave forcing at Narrabeen, Australia. *Scientific Data*. 2016;3. Article number: 160024
- [26] Chu Z, Yang X, Feng X, Fan D, Li Y, Shen X, et al. Temporal and spatial changes in coastline movement of the Yangtze delta during 1974-2010. *Journal of Asian Earth Sciences*. 2013;66:166-174
- [27] Liu Y, Huang H, Qiu Z, Fan J. Detecting coastline change from satellite images based on beach slope estimation in a tidal flat. *International Journal of Applied Earth Observation and Geoinformation*. 2013;23:165-176
- [28] Yu K, Hu C, Muller-Karger FE, Lu D, Soto I. Shoreline changes in west-Central Florida between 1987 and 2008 from Landsat observations. *International Journal of Remote Sensing*. 2011;32(23):8299-8313
- [29] Kuleli T, Guneroglu A, Karsli F, Dihkan M. Automatic detection of shoreline change on coastal Ramsar wetlands of Turkey. *Ocean Engineering*. 2011;38(10):1141-1149
- [30] Almonacid-Caballer J, Sánchez-García E, Pardo-Pascual JE, Balaguer-Beser AA, Palomar-Vázquez J. Evaluation of annual mean

shoreline position deduced from Landsat imagery as a mid-term coastal evolution indicator. *Marine Geology*. 2016;**372**:79-88

[31] Li W, Gong P. Continuous monitoring of coastline dynamics in western Florida with a 30-year time series of Landsat imagery. *Remote Sensing of Environment*. 2016;**179**:196-209

[32] Davidson MA, Turner IL. A behavioral template beach profile model for predicting seasonal to interannual shoreline evolution. *Journal of Geophysical Research: Earth Surface*. 2009;**114**(F1)

[33] Ruessink BG, Coco G, Ranasinghe R, Turner IL. Coupled and noncoupled behavior of three-dimensional morphological patterns in a double sandbar system. *Journal of Geophysical Research: Oceans*. 2007;**112**(C7)

[34] Boak L, McGrath J, Jackson A. IENCE—A case study—The Northern Gold Coast Beach protection strategy. *Coastal Engineering. Proceedings of the 27th International Conference on Coastal Engineering*. 2000;**4**:3710-3717

[35] Blacka MJ, Anderson DJ, Lopez LM. Analysis of shoreline variability, seasonality and erosion/accretion trends: February–July 2008. Report 18. Northern Gold Coast coastal imaging system. WRL Technical Report. November 2008

[36] Aarninkhof S, Roelvink J, editors. *Argus-Based Monitoring of Intertidal Beach Morphodynamics*. Coastal Sediments. ASCE. Proceedings of Coastal Sediments. New York: American Society of Civil Engineers; 1999;**99**: 2429-2444

[37] Davidson MA, Lewis RP, Turner IL. Forecasting seasonal to multi-year shoreline change. *Coastal Engineering*. 2010;**57**(6):620-629

[38] Mishra N, Haque M, Leigh L, Aaron D, Helder D, Markham B. Radiometric cross calibration of Landsat 8 operational land imager (OLI) and Landsat 7 enhanced thematic mapper plus (ETM+). *Remote Sensing*. 2014;**6**(12):12619

[39] Splinter KD, Carley JT, Golshani A, Tomlinson R. A relationship to describe the cumulative impact of storm clusters on beach erosion. *Coastal Engineering*. 2014;**83**:49-55